Group-wise Cortical Correspondence via Sulcal Curve-Constrained Entropy Minimization

Ilwoo Lyu[1], Sun Hyung Kim[2], Joon-Kyung Seong[4], Sang Wook Yoo[5], Alan C. Evans[6], Yundi Shi[2], Mar Sanchez[7], Marc Niethammer[1,3], and Martin A. Styner[1,2]

[1] Dept. of Computer Science, University of North Carolina, Chapel Hill, NC, USA
{ilwoolyu,styner}@cs.unc.edu
[2] Dept. of Psychiatry, University of North Carolina, Chapel Hill, NC, USA
[3] BRIC, University of North Carolina, Chapel Hill, NC, USA
[4] Dept. of Biomedical Engineering, Korea University, Seoul, South Korea
[5] Dept. of Computer Science, KAIST, Daejeon, South Korea
[6] Montreal Neurological Institute, McGill University, Montreal, Quebec, Canada
[7] Yerkes National Primate Research Center, Emory University, Atlanta, GA, USA

Abstract. We present a novel cortical correspondence method employing group-wise registration in a spherical parametrization space for the use in local cortical thickness analysis in human and non-human primate neuroimaging studies. The proposed method is unbiased registration that estimates a continuous smooth deformation field into an unbiased average space via sulcal curve-constrained entropy minimization using spherical harmonic decomposition of the spherical deformation field. We initialize a correspondence by our pair-wise method that establishes a surface correspondence with a prior template. Since this pair-wise correspondence is biased to the choice of a template, we further improve the correspondence by employing unbiased ensemble entropy minimization across all surfaces, which yields a deformation field onto the iteratively updated unbiased average. The specific entropy metric incorporates two terms: the first focused on optimizing the correspondence of automatically extracted sulcal landmarks and the second on that of sulcal depth maps. We also propose an encoding scheme for spherical deformation via spherical harmonics as well as a novel method to choose an optimal spherical polar coordinate system for the most efficient deformation field estimation. The experimental results show evidence that the proposed method improves the correspondence quality in non-human primate and human subjects as compared to the pair-wise method.

Keywords: Group-wise correspondence, Sulcal curves, Spherical harmonics, Entropy minimization, Cortical thickness

1 Introduction

Group analysis of cortical properties such as cortical thickness is an important task for monitoring brain growth, investigating anatomic connectivity, and discovering cortical disease patterns. A prerequisite to such tasks is to establish a

consistent cortical correspondence across a population of subject cortices. However, the high variability of the cortical folding patterns provides a significant challenge to the computation of such an inter-subject cortical correspondence over the entire cortical surface.

There have been two main approaches to the cortical correspondence computation that are based either on volume images or on cortical surface models. As recently reported in [3], a cortical correspondence is more likely to be enhanced via surface registration on a cortical surface model due to its geometric property preservation of the cortex, while volume-based registration approaches using only image intensities are hard to sufficiently characterize the cortical regions for a localized vertex or voxel-wise analysis. Moreover, since the choice of invariant features across a population is essential for a consistent correspondence, folding patterns along central sulcal fundic regions can be used as features due to their relative reduced variability. Studies on sulcal region recognition and folding patterns were presented in [8,13,7].

Several researchers proposed cortical registration via a spherical mapping to the template space in a pair-wise registration manner [15,2,10]. In [5], an iterative registration scheme was introduced, which updates the initial template for better correspondence establishment. The study presented by Van Essen [14] even applied to non-human primate subjects. Lyu et al. [6] also proposed a spherical mapping that uses spherical harmonic decomposition for correspondence extrapolation by taking advantage of its convenient, global representation of the deformation field. In general, however, these pair-wise registration methods are inherently biased to the template surface, which is undesirable for the group analysis purpose.

To take account of variance of the cortical properties over pair-wise methods, Cates et al. [1] proposed particle-based registration on cortical surface models without using a template model or prior information. Later, Oguz et al. [9] further enhanced the particle-based registration by incorporating curvature features, showing the improved correspondence via the analyses of cortical thickness over the entire cortical surface. However, these methods did not incorporate gyral/sulcal patterns nor did they provide explicit estimation of a deformation field between subjects, rather with a particle-based correspondence that implicitly defines a deformation model without guarantee of topology preservation.

In this paper, we propose a fully automatic group-wise cortical correspondence method evaluated on both macaque and human cortical surfaces. We initially compute a pair-wise correspondence to the given template surface and further improve the correspondence across a population via ensemble entropy minimization without employing any template surface. In particular, we use spherical harmonic decomposition to continuously represent the correspondence over the entire cortical surface by using a metric that incorporates errors over sulcal landmarks and sulcal depth maps. We also propose a novel spherical polar coordinate system to avoid a distorted representation of the deformation field. In summary, the main novelties presented here are: 1) group-wise cortical correspondence using an explicit deformation field, 2) optimal pole selection for a
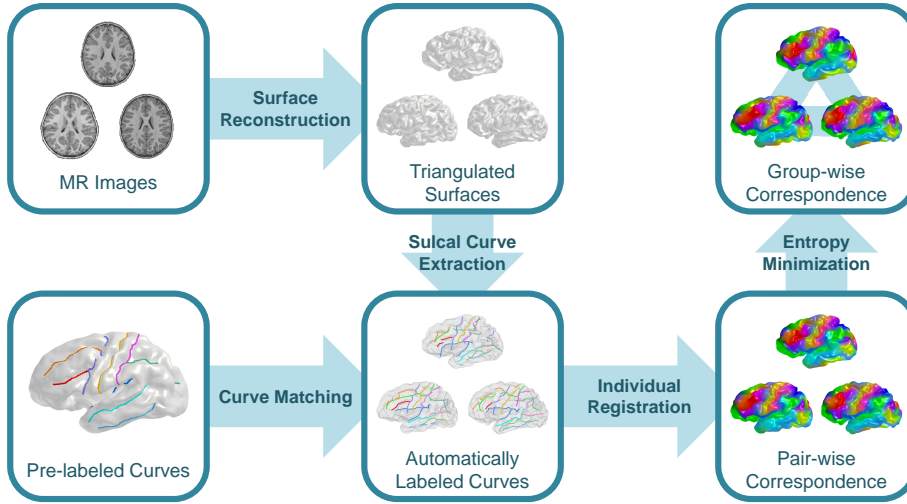
Fig. 1. Schematic overview of the proposed method

smooth deformation field representation, and 3) application in both non-human primate and human data. Figure 1 illustrates an overview of our pipeline.

2   Method

2.1   Preprocessing

Surface Reconstruction. Raw MR images are registered into the standard-ized stereotaxic space using a rigid transformation. The registered images are corrected for intensity nonuniformity resulting from inhomogeneities in the magnetic field. The inner- and outer-surfaces are automatically extracted by the Con-strained Laplacian-based Automated Segmentation with Proximities (CLASP) algorithm [4]. We use the middle cortical surface models with a triangulated mesh of 40,962 vertices in the native space. Each vertex of the surface models is then homeomorphically transformed onto the common unit sphere using a deformable surface model [4]. After surface reconstruction, we compute sulcal depth maps via the geodesic distance from the gyral crowns as proposed in [12].

Landmark Correspondence. We use automatic sulcal curve extraction [13] and automatic sulcal curve labeling [7] to extract a set of labeled sulcal curves. In particular, the unlabeled sulcal curves (consisting of ordered sets of points) are extracted from the triangulated surface, and then pre-labeled sulcal curves in the template are employed to label matched (corresponding) sulcal curves in the subject, while discarding minor and extraneous curves. This labeling method further establishes a point-by-point correspondence across these sulcal curves called sulcal landmarks in the remainder of this paper.

2.2   Sulcal Curve-Constrained Pair-wise Correspondence

Problem Definition. For two given triangulated cortical surfaces (template and subject), we denote V_{temp} and V_{subj} as the sets of the vertices of the template and subject surfaces. Our goal is to estimate a continuous mapping function of the cortical correspondence $M : \mathbb{R}^3 \to \mathbb{R}^3$ such that

$$u = M(v) \ , \tag{1}$$

where $u \in V_{\text{temp}}$ and $v \in V_{\text{subj}}$ are the corresponding points.

Consistent Displacement Encoding Scheme. To take advantage of the well-known spherical parametrization, we map all vertices of the cortical surfaces onto the common unit sphere by using an invertible spherical mapping $\psi : \mathbb{R}^3 \to \mathbb{S}^2$ established in the preprocessing stage. Note that this spherical mapping generally does not establish an appropriate correspondence. We then locally encode the deformation as change in local spherical polar angles of elevation $\Delta\theta$ and azimuth $\Delta\phi$. It can be easily observed that the same length of geodesic distances provides different angular differences close to the equator as compared to closer to the pole. To avoid such inconsistency and thus to provide a consistent arclength encoding, we propose a locally normalized coordinate system. For this local normalization, let $\psi_{\text{temp}}(p)$ and $\psi_{\text{subj}}(q)$ be the mapped corresponding sulcal landmarks from the template and a subject, respectively. First, we find a rotation matrix $\mathbf{R}_q$ with an angle ($\leq 90°$) along the longitude circle passing through $\psi_{\text{subj}}(q)$ and the two poles, such that $\psi_{\text{subj}}(q)$ is exactly located on the equator. By applying $\mathbf{R}_q$ to $\psi_{\text{temp}}(p)$ and $\psi_{\text{subj}}(q)$, we then compute normalized angular displacements $\Delta\theta$ and $\Delta\phi$. As sulcal landmarks are described by spherical polar coordinates, we denote an operator $\odot$ that rotates these landmarks with a rotation matrix defined in a Cartesian coordinate system. Thus, the local landmark displacement at a point i (θ_i, ϕ_i) on the unit sphere is represented as a vector $\mathbf{d}_i = \mathbf{R}_{q_i} \odot \psi_{\text{temp}}(p_i) - \mathbf{R}_{q_i} \odot \psi_{\text{subj}}(q_i) = [\Delta\theta_i, \Delta\phi_i]^T$ (see Fig. 2a).

Initial Deformation Field. To find an initial deformation field of the entire surface, we compute least squares fitting of spherical harmonics to displacements of the sulcal landmarks established in the sulcal labeling step. This fitting is standard spherical harmonic decomposition of the spherical signals ($\Delta\theta$ and $\Delta\phi$). At a point (θ, ϕ) on the sphere, the spherical harmonic basis function of degree l and order m $(-l \leq m \leq l)$ is given by

$$Y_l^m(\theta, \phi) = \sqrt{\frac{2l+1}{4\pi} \frac{(l-m)!}{(l+m)!}} P_l^m(\cos\theta)e^{im\phi} \ , \tag{2}$$

$$Y_l^{-m}(\theta, \phi) = (-1)^m Y_l^{m*}(\theta, \phi) \ , \tag{3}$$

where Y_l^{m*} denotes the complex conjugate of Y_l^m and P_l^m is the associated Legendre polynomial

$$P_l^m(x) = \frac{(-1)^m}{2^l l!}(1 - x^2)^{\frac{m}{2}} \frac{d^{(l+m)}}{dx^{(l+m)}}(x^2 - 1)^l \ . \tag{4}$$

$$\mathbf{d}_i = [\Delta\theta_i, \Delta\phi_i]^T$$

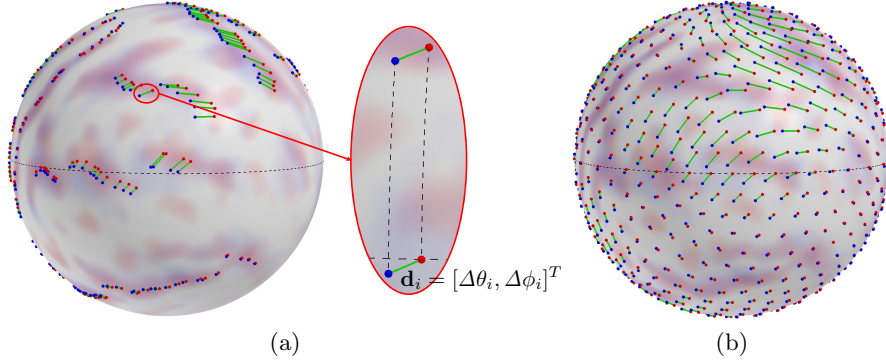(a)   (b)

Fig. 2. Displacement encoding (a) and estimated deformation field (sampling of a continuous representation) with sulcal depth maps (b). A spherical displacement is encoded as change in spherical angles after rotation onto the equator for arclength preservation, which avoids a distorted displacement representation. The deformation field is estimated by extrapolation using spherical harmonic decomposition.

Since the spherical harmonic basis functions are defined in the complex domain, we use a real form of the functions defined by

$$Y_{l,m} = \begin{cases} \frac{1}{\sqrt{2}}(Y_l^m + (-1)^m Y_l^{-m}) & m > 0 \, , \\ Y_l^0 & m = 0 \, , \\ \frac{1}{\sqrt{2}i}(Y_l^{-m} - (-1)^m Y_l^m) & m < 0 \, . \end{cases} \tag{5}$$

Given spherical harmonic decomposition of degree k, we have $(k+1)^2$ spherical harmonic basis functions at a given point on the sphere. To avoid a rank deficient problem, we assume that the number of the landmarks n is larger than $(k+1)^2$. The coefficients can then be estimated by standard least squares fitting:

$$\mathbf{C} = \left(\mathbf{YY^T}\right)^{-1}\mathbf{YD^T} \, , \tag{6}$$

where $\mathbf{D} = [\mathbf{d}_1, \mathbf{d}_2, \cdots, \mathbf{d}_n]$ and $\mathbf{Y}$ is a $(k+1)^2$-by-n matrix that incorporates the spherical harmonic basis functions. Once the coefficients of the spherical harmonic decomposition are determined, for $\forall v \in V_{\text{subj}}$, its deformed position in the template space is easily reconstructed by the mapping function $\hat{M}$:

$$\hat{u} = \hat{M}(v) = \psi_{\text{temp}}^{-1}(\mathbf{R}_v^T \odot (\mathbf{R}_v \odot \psi_{\text{subj}}(v) + \mathbf{C}^T \cdot \mathbf{Y}_v)) \, , \tag{7}$$

where $\mathbf{Y}_v$ is a column vector of the spherical harmonic basis functions at $\psi_{\text{subj}}(v)$ and $\mathbf{R}_v$ is a rotation matrix that puts $\psi_{\text{subj}}(v)$ on the equator. Figure 2b shows an example of the estimated deformation field.

This spherical harmonic decomposition of the deformation field is hierarchical and orthonormal. We employ the hierarchy in that the initial deformation field is computed via low degree ($k = 5$) fitting of sulcal landmarks and higher degree representations are used in the optimization stage.

Optimization. Since the initial coefficients are determined only by sulcal landmarks, the cortical correspondence is potentially biased to the specific sulcal fundic regions selected in the sulcal labeling step as well as affected by minor mislabeling errors. For improved correspondence establishment, we further formulate a metric that incorporates sulcal landmark errors and differences between sulcal depth maps via normalized cross correlation over the entire cortical surface. To regularize the impact of sulcal landmark errors, we define a weighting function f under the Gaussian assumption. Specifically, incorporating $d_{\min}$ as voxel size, sulcal landmark errors below $d_{\min}$ are ignored and have the maximum at distance $d_{\max}$, chosen 10–20 times larger than $d_{\min}$, as follows.

$$f(d) = 2 \int_{d_{\min}}^{d} \frac{I(d)}{\sigma\sqrt{2\pi}} \exp\left\{ -\frac{1}{2} \left(\frac{x - d_{\min}}{\sigma} \right)^2 \right\} dx \;, \qquad (8)$$

$$I(d) = \begin{cases} 1 & d \geq d_{\min} \;, \\ 0 & \text{otherwise} \;, \end{cases} \qquad (9)$$

where $6 \cdot \sigma = d_{\max} - d_{\min}$. Now, we define $L(\cdot, \cdot) = f(\eta \cdot \operatorname{arclen}(\cdot, \cdot))$ as a regularized arclength, where η is a ratio of the geodesic distance between two points on the unit sphere and on the template surface. In practice, it can be approximated by a ratio of the triangle size under the assumption that the template surface consists of uniform triangles. The resulting overall cost function like an M-estimator is thus formulated with a regularization factor w by letting an operator $\otimes$ denote the normalized cross correlation between two sulcal depth maps:

$$\hat{\mathbf{C}} = \operatorname*{argmin}_{\mathbf{C}} \left[w \left\{ \frac{1}{n} \sum_{i=1}^{n} L(p_i, \hat{p}_i) \right\} + (1 - w) \left\{ \frac{1}{2} \left(1 - S(\{u\}) \otimes S(\{\hat{u}\}) \right) \right\} \right] \;, \qquad (10)$$

where $S(\cdot)$ is a sulcal depth map reconstructed from a set of vertices. The optimization procedure employs the NEWUOA optimizer [11] for minimizing $\mathbf{C}$. In our experiment, we empirically set $w = 0.5$.

Optimal Pole Selection. The proposed spherical polar coordinate system does not force the direction of displacements to be invariant to locations. Depending on rotation to the equator, two identical displacements are likely to have a different sign in polar angles if they are computed on opposite sites with respect to the pole. This can yield a deformation field with abrupt sign changes close to the pole. A proper choice of the pole $\mathbf{e}$ can significantly minimize this issue and yield smooth deformation fields. The presence of non-smooth deformation will generally lead to high magnitude coefficients in the high-frequency harmonic basis functions. Based on this observation, we employ a coefficient sum-based metric that weighs higher frequency coefficients stronger:

$$\hat{\mathbf{e}} = \operatorname*{argmin}_{\mathbf{e}} \sum_{l=0}^{k} \sum_{m=-l}^{l} (l + 1) \cdot \left(|c_{\theta_{l,m}}| + |c_{\phi_{l,m}}| \right) \;, \qquad (11)$$

where c_θ and c_ϕ are coefficients for elevation and azimuth displacements. As this metric possibly has local minima, we initialize the optimization with multiple initial guesses spread across the sphere and select the minimum as the final pole.

2.3   Extension to Group-wise Correspondence

While our pair-wise method provides adequate registration results (see Sect. 3), we propose here the use of group-wise registration to further improve these results as well as to remove the template selection bias inherent to pair-wise registration. A group-wise correspondence is computed independently from the template and thus is expected to perform more stably across a population of surfaces. We propose to use entropy minimization to establish a group-wise correspondence. Our group-wise correspondence method incorporates entropy terms computed over the landmark distribution and sulcal depth maps.

Problem Definition. For N given triangulated cortical surfaces mapped onto the unit sphere, each of which has the same number n of the common corresponding points, we let V^i be the set of the vertices in the ith subject, $i = 1, \cdots, N$. The goal is to estimate continuous mapping functions of the cortical correspondence $M_i : \mathbb{S}^2 \to \mathbb{S}^2$ across subjects such that

$$M_1(v^1) = M_2(v^2) = \cdots = M_N(v^N) \, , \tag{12}$$

where $v^i \in V^i$ are the corresponding points across subjects. Let $\mathbf{x}(M_j)$ be a column vector of the corresponding points of a subject j deformed by M_j, i.e., $\mathbf{x}(M_j) = [M_j(v_1^j), \cdots, M_j(v_n^j)]^T$. As described in [9], we assume that $\mathbf{x}(M_j)$ are instances of $\mathbf{X}$ drawn from a probability density function. The amount of the information in the random sampling is given by the entropy $H[\mathbf{X}]$, and the minimization problem is then formulated as follows.

$$\{\hat{M}_1, \cdots, \hat{M}_N\} = \operatorname*{argmin}_{\{M_1, \cdots, M_N\}} H[\mathbf{x}] \, , \tag{13}$$

which drives mapped/deformed corresponding points closer to each other.

Entropy of Landmark Errors. We employ the pair-wise correspondence (Sect. 2.2) as initialization for the proposed group-wise method. As the sulcal labeling procedure yields varying parts of sulcal curves being labeled, we constrain the set of sulcal landmarks only those that have a full correspondence across all cortical surfaces. A key step for entropy computation is the density estimation of corresponding sulcal landmarks. However, appropriate density estimation on the sphere can be computationally demanding since it involves geodesic distance computation. Similar to [9] for efficiency, we assume that the initial mapping well centralizes corresponding sulcal landmarks, which allows a mapping from the spherical space to the Euclidean space $\mathbb{S}^2 \to \mathbb{R}^3$ under the assumption of the proximity of the landmarks. We compute the average over corresponding sulcal landmarks, which is rescaled to the sphere, and the landmarks are projected onto the tangential plane at that approximated mean to enable Euclidean statistics.

Entropy of Sulcal Depth. Since sulcal landmarks are sparsely distributed over the sphere and also likely possess minor mislabeling, we employ additional entropy computation over sulcal depth maps densely sampled across the surface. Let $s(\cdot)$ denote the sulcal depth at a given point and v^j be the point in the jth subject such that $u = M_j(v^j)$, where u is a given point on the sphere. Given M_j, v^j has a correspondence with its corresponding points. Ideally, there will be little difference in sulcal depth across the corresponding points if the mapping is well established, that is, $s(M_1(v^1)) \cong \cdots \cong s(M_N(v^N))$. By uniform icosahedron subdivision-based spherical sampling of u, sulcal depth agreement is straightforwardly plugged into the entropy minimization problem.

Entropy Minimization. We model $\mathbf{x}(M_j)$ as an instance of $\mathbf{X}$ such that

$$\mathbf{x}(M_j) = \left[proj_{\bar{v}_1}(M_j(v_1^j)), \cdots, proj_{\bar{v}_n}(M_j(v_n^j)), S(\{M_j(v^j)\}) \right]^T, \qquad (14)$$

where $proj_{\bar{v}}(\cdot)$ denotes the projection of a point onto the tangential plane at the approximated mean $\bar{v}$ over the corresponding sulcal landmarks. For the density estimation, we assume a multivariate Gaussian distribution with covariance Σ and therefore, the entropy is obtained by

$$H[\mathbf{X}] \approx \frac{1}{2} \ln |\Sigma| = \frac{1}{2} \sum \ln \lambda, \qquad (15)$$

where λ are the eigenvalues of Σ. By letting $\bar{\mathbf{x}}$ be the sample mean and $\mathbf{Z} = [\mathbf{x}(M_1) - \bar{\mathbf{x}}, \cdots, \mathbf{x}(M_N) - \bar{\mathbf{x}}]$, the sample covariance is given by $\frac{1}{N-1}\mathbf{Z}\mathbf{Z}^T$. In practice, however, the eigendecomposition of the sample covariance is an intractable task for the large dimension of $\mathbf{X}$ ($\gg N$). As stated in [9], we instead compute the eigenvalues of $\frac{1}{N-1}\mathbf{Z}^T\mathbf{Z}$ in the dual space. The optimization uses the NEWUOA optimizer [11] for solving the entropy cost function.

3   Experimental Results

We applied the proposed method on both non-human primate and human subjects to evaluate the established correspondence quality. Since there exists no ground-truth of the cortical correspondence, we made comparisons with the initial spherical mapping and the pair-wise method via analysis on cortical thickness as well as the agreement with manually labeled sulcal curves.

3.1   Macaque Cortical Surfaces

We used the same data set as that in [6]. 18-month-old macaques were imaged under anesthesia at the Yerkes Imaging Center (Emory University, GA) on a 3T Siemens Trio scanner with an 8-channel phase array trans-receiving volume coil. T_1-weighted scans were acquired using a 3D MP-RAGE sequence with GRAPPA at a high resolution of $0.6\,mm \times 0.6\,mm \times 0.6\,mm$ (TR $= 3{,}000\,ms$,
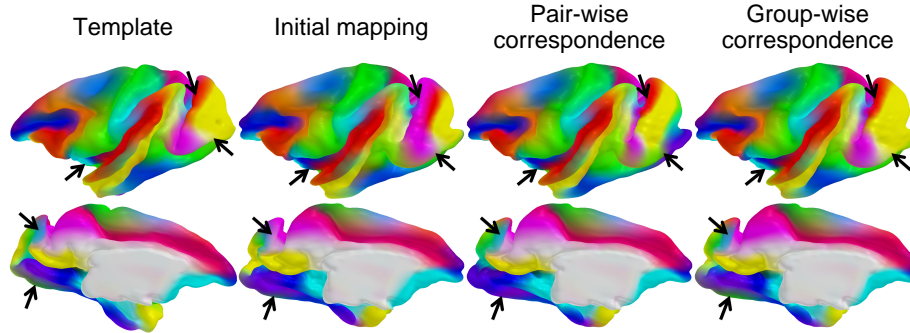
Fig. 3. Visual comparison of correspondence results. The colored template surface (*first column*) is propagated to a selected, representative example surface via initial spherical mapping (*second*), pair-wise correspondence (*third*), and group-wise correspondence (*fourth*). The arrows indicate areas of visual differences across the correspondence methods.

TE $= 3.33\,ms$, flip angle $= 8°$, matrix $= 192 \times 192$). In the experiment, we randomly selected a single subject as a template with its 11 manually labeled sulcal curves: central sulcus, arcuate sulcus, principal sulcus, superior temporal sulcus, intraparietal sulcus, lunate sulcus, inferior occipital sulcus, occipitotemporal sulcus, cingulate sulcus, parieto-occipital fissure, and sylvian fissure.

We further established a sulcal curve-based color mapping across the cortical surfaces to provide a visual quality assessment of the established correspondence by propagation of the colorized template surface to other subjects. To generate the reference colorized surface, a unique RGB color was assigned to each sulcal curve, and then each RGB channel was extrapolated to the entire surface via spherical harmonic decomposition. In Fig. 3, the proposed group-wise method shows qualitative improvement over the pair-wise correspondence.

3.2   Human Cortical Surfaces

Pediatric 2-year-old subjects were acquired on a 3T Siemens Trio scanner at a resolution of $1.0\,mm \times 1.0\,mm \times 1.0\,mm$ with T_1-(160 slices, TR $= 2400\,ms$, TE $= 3.16\,ms$, flip angle $= 8°$, matrix $= 256 \times 256$) and T_2-weighted (160 slices, TR $= 3200\,ms$, TE $= 499\,ms$, flip angle $= 120°$, matrix $= 256 \times 256$) scans. We used 10 subjects chosen at random from the scans acquired as part of the Infant Brain Imaging Study (IBIS) network[1] at four different sites (University of North Carolina, University of Washington, Washington University in Saint Louis, and The Children's Hospital of Philadelphia). We randomly selected a single subject as a template, and an expert manually labeled 13 major curves on the template surface: superior temporal sulcus (STS), inferior temporal sulcus (ITS), collateral sulcus (ColS), central sulcus (CS), precentral sulcus (PrCS), postcentral sulcus
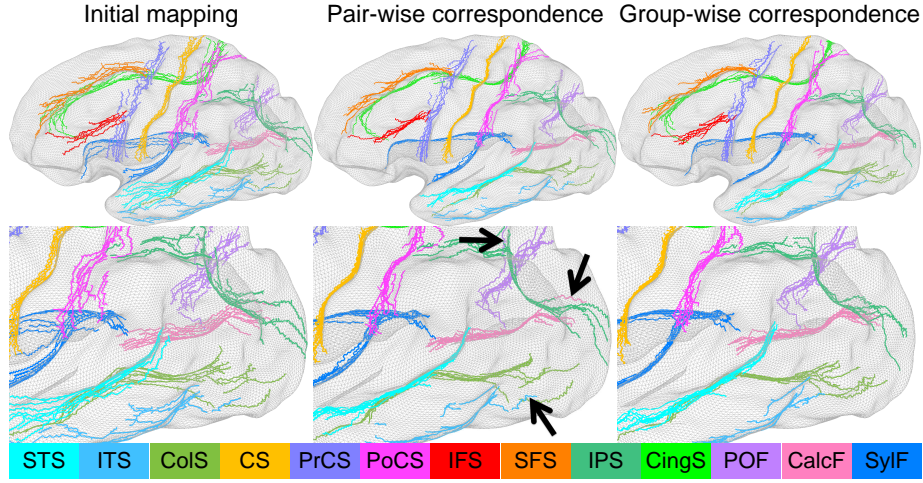
---

[1] http://www.ibis-network.org

Fig. 4. Sulcal curve agreement by initial spherical mapping (*left*), pair-wise correspondence (*middle*), and group-wise correspondence (*right*). The arrows indicate improved agreement in the group-wise as compared to the pair-wise correspondence.

(PoCS), inferior frontal sulcus (IFS), superior frontal sulcus (SFS), intraparietal sulcus (IPS), cingulate sulcus (CingS), parieto-occipital fissure (POF), calcarine fissure (CalcF), and sylvian fissure (SylF) (see Fig. 4). Only left hemispheres were used in the experiment. For a visual assessment, all major curves were also manually labeled on the 9 remaining subjects.

We applied a leave-one-out cross-validation technique for evaluation of the optimal pole selection. We removed a single sulcus from each individual subject during registration and measured landmark (reconstruction) errors between the removed sulcus reconstructed by the deformation field and its corresponding one in the template. Figure 5 shows the smaller average reconstruction errors for the optimal pole and the reduced coefficient load of the azimuth displacement for the high-frequency harmonic basis functions by the proposed pole selection.

For quantitative evaluation of the correspondence quality, we first measured cross-subject variance estimates of sulcal depth over all vertices of the entire surface across subjects. However, such an evaluation is biased, as sulcal depth is employed in the cost function. We further used variance estimates of cortical thickness as well as a visual assessment of manually labeled sulcal curves for unbiased evaluation. Note that the manually labeled sulcal curves were not used during processing in our pipeline, which implies that the evaluation is independent of the automatically labeled curves. In Table 1 the statistical analysis indicates superior performance of our method for variance of sulcal depth and cortical thickness measures, with significant differences to both the initial mapping and the pair-wise method, revealed by Student's t-test ($p < 0.0001$). Visually, the mapped major sulcal curves shows improved agreement in several regions as compared to the pair-wise correspondence as shown in Fig. 4.
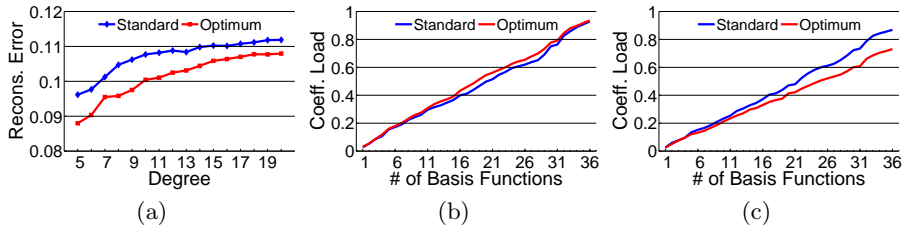
Fig. 5. Reconstruction errors (a) and cumulative coefficient load for elevation (b) and azimuth (c) displacements. No major differences are observed for the elevation displacements, whereas for the azimuth displacements, the total amount of the coefficient load significantly decreases for the optimal pole selection.

Table 1. Statistical analysis of variance of cortical properties. The proposed method shows better variance estimates of sulcal depth and of cortical thickness with significant differences to both the initial mapping and the pair-wise method ($p < 0.0001$).

	Sulcal Depth (mm^2)		Cortical Thickness (mm^2)	
Method	Mean	SD	Mean	SD
Initial	1.9234	1.1300	0.5003	0.3925
Pair-wise	1.5014	0.9759	0.4948	0.3799
Group-wise	**1.3181**	**0.9446**	**0.4741**	**0.3616**

4   Conclusion

We presented an automatic group-wise cortical correspondence method that estimates a smooth continuous deformation field using entropy minimization of sulcal landmarks and sulcal depth maps. In our experiment, the proposed method outperformed the pair-wise method in non-human subjects via a visual assessment and in human subjects via quantitative analysis and visual comparisons. To enable enhanced spherical harmonic decomposition of the deformation field, we also proposed a consistent displacement encoding scheme and an optimal pole selection strategy. In the experiment, the optimal pole selection showed smaller reconstruction errors and more efficient encoding of the deformation field.

The proposed method allows the inclusion of additional information such as DTI-based connectivity akin to [9]. Furthermore, any prior information such as lobar labeling, surface colorization, etc. can be straightforwardly propagated from the template. In this way, inter-subject variability of cortical properties defined in the template space could be incorporated into the entropy minimization.

It is noteworthy that our proposed method is sensitive to the quality of the automatic labeling of sulcal curves, as mislabeled sulcal curve will negatively influence the established correspondence. In our experiment, the proposed method has (qualitatively) shown to be quite resilient to errors in sulcal labeling if the large majority of sulcal curves within the same class are correctly identified. In our future work, we will extend this method to include robust estimators of entropy for the sulcal curves to reduce the influence of such errors.

References

1. Cates, J., Fletcher, P., Styner, M., Shenton, M., Whitaker, R.: Shape modeling and analysis with entropy-based particle systems. In: Karssemeijer, N., Lelieveldt, B. (eds.) IPMI 2007. LNCS, vol. 4584, pp. 333–345. Springer, Heidelberg (2007)
2. Davies, R., Twining, C., Cootes, T., Taylor, C.: Building 3-d statistical shape models by direct optimization. IEEE Trans. Med. Imaging 29(4), 961–981 (2010)
3. Du, J., Younes, L., Qiu, A.: Whole brain diffeomorphic metric mapping via integration of sulcal and gyral curves, cortical surfaces, and images. NeuroImage 56(1), 162–173 (2011)
4. Kim, J., Singh, V., Lee, J., Lerch, J., Ad-Dab'bagh, Y., MacDonald, D., Lee, J., Kim, S., Evans, A.: Automated 3-d extraction and evaluation of the inner and outer cortical surfaces using a laplacian map and partial volume effect classification. NeuroImage 27(1), 210–221 (2005)
5. Lyttelton, O., Boucher, M., Robbins, S., Evans, A.: An unbiased iterative group registration template for cortical surface analysis. NeuroImage 34(4), 1535–1544 (2007)
6. Lyu, I., Kim, S., Seong, J., Yoo, S., Evans, A., Shi, Y., Sanchez, M., Niethammer, M., Styner, M.: Cortical correspondence via sulcal curve-constrained spherical registration with application to macaque studies. In: Ourselin, S., Haynor, D. (eds.) Medical Imaging 2013: Image Processing. vol. 8669, pp. 86692X–1–7. SPIE (2013)
7. Lyu, I., Seong, J., Shin, S., Im, K., Roh, J., Kim, M., Kim, G., Kim, J., Evans, A., Na, D., Lee, J.: Spectral-based automatic labeling and refining of human cortical sulcal curves using expert-provided examples. NeuroImage 52(1), 142–157 (2010)
8. Mangin, J., Riviere, D., Cachia, A., Duchesnay, E., Cointepas, Y., Papadopoulos-Orfanos, D., Scifo, P., Ochiai, T., Brunelle, F., Régis, J.: A framework to study the cortical folding patterns. NeuroImage 23, S129–S138 (2004)
9. Oguz, I., Niethammer, M., Cates, J., Whitaker, R., Fletcher, T., Vachet, C., Styner, M.: Cortical correspondence with probabilistic fiber connectivity. In: Prince, J., Pham, D., Myers, K. (eds.) IPMI 2009. LNCS, vol. 5636, pp. 651–663. Springer, Heidelberg (2009)
10. Park, H., Park, J., Seong, J., Na, D., Lee, J.: Cortical surface registration using spherical thin-plate spline with sulcal lines and mean curvature as features. Journal of Neuroscience Methods 206(1), 46–53 (2012)
11. Powell, M.: The newuoa software for unconstrained optimization without derivatives. Large-Scale Nonlinear Optimization 83, 255–297 (2006)
12. Robbins, S.: Anatomical standardization of the human brain in euclidean 3-space and on the cortical 2-manifold. Ph.D. thesis, McGill University (2004)
13. Seong, J., Im, K., Yoo, S., Seo, S., Na, D., Lee, J.: Automatic extraction of sulcal lines on cortical surfaces based on anisotropic geodesic distance. NeuroImage 49(1), 293–302 (2010)
14. Van Essen, D.: Surface-based approaches to spatial localization and registration in primate cerebral cortex. NeuroImage 23, S97–S107 (2004)
15. Yeo, B., Sabuncu, M., Vercauteren, T., Ayache, N., Fischl, B., Golland, P.: Spherical demons: Fast diffeomorphic landmark-free surface registration. IEEE Trans. Med. Imaging 29(3), 650–668 (2010)